frontiers | Frontiers in Materials

TYPE Original Research
PUBLISHED 04 October 2022
DOI 10.3389/fmats.2022.933749

OPEN ACCESS

EDITED BY
Emilio Isaac Alarcon,
University of Ottawa, Canada

REVIEWED BY
Nemany A. N. Hanafy,
Kafrelsheikh University, Egypt
Alessandra Quarta,
Institute of Nanotechnology (CNR), Italy

*CORRESPONDENCE
Myla Santiago-Bautista,
mrsantiago@ust.edu.ph

SPECIALTY SECTION
This article was submitted to Biomaterials and Bio-Inspired Materials, a section of the journal Frontiers in Materials

RECEIVED 01 May 2022
ACCEPTED 08 September 2022
PUBLISHED 04 October 2022

CITATION
Repotente EC, Carreon AJ, Devanadera MK, Esmalla MS and Santiago-Bautista M (2022), Cytotoxic potential on human breast and lung cancer cells of the biosynthesized gold nanoparticles from the reduction of chloroauric acid by lactic acid isolated from Lactobacillus acidophilus. *Front. Mater.* 9:933749. doi: 10.3389/fmats.2022.933749

Cytotoxic potential on human breast and lung cancer cells of the biosynthesized gold nanoparticles from the reduction of chloroauric acid by lactic acid isolated from *Lactobacillus acidophilus*

Elmer Casley Repotente Jr[1], Angelo Jose Carreon[1], Mark Kevin Devanadera[1,2,3], Maria Salvacion Esmalla[1] and Myla Santiago-Bautista[1,3]*

[1]Department of Biochemistry, Faculty of Pharmacy, University of Santo Tomas, Manila, Philippines, [2]The Graduate School, University of Santo Tomas, Manila, Philippines, [3]Mammalian Tissue Culture Laboratory, Research Center for the Natural and Applied Sciences, University of Santo Tomas, Manila, Philippines

Chemotherapy side effects, drug resistance, and tumor metastasis hinder the progress of cancer treatments, which has led to cancer patients having a poor prognosis. In recent years, nanoparticles (NPs) have become an emerging trend in drug delivery technology. The biosynthesis of gold nanoparticles (AuNPs) from lactic acid as probiotic metabolites is a cost-efficient and eco-friendly approach due to the widespread availability and ease of culturing methods. Here, AuNPs were synthesized by reducing chloroauric acid using lactic acid isolated from the probiotic *Lactobacillus acidophilus*. Surface characterization of the biosynthesized gold nanoparticles was performed by UV-visible spectroscopy, field emission scanning electron microscopy with energy dispersive spectroscopy (FESEM-EDS), and atomic force microscopy (AFM). The distinct peak of the AuNPs in the UV-Vis spectra at around 520 nm indicates the nanoscale level of the gold particles. SEM images of the shape of the biosynthesized AuNPs were found to be small, smooth spherical particles with sizes ranging from 6 to 12 nm. AFM results agree with SEM images, showing AuNPs with sizes ranging from 4 to 15 nm. The anticancer activities of the biosynthesized AuNPs have been investigated by cytotoxicity (MTT) and apoptosis (Caspase 3/7) assay in the human breast and lung cancer cells (MCF7 and A549), and control (myoblasts). MTT assay showed AuNPs' cytotoxic potential on cancer cells (MCF7 and A549) compared to normal cells (myoblasts). Cytotoxicity and apoptosis assay of the synthesized AuNPs exhibit toxicity against human breast adenocarcinoma cells (MCF7, IC_{50} of 0.075 mM) and human lung cancer cells (A549, IC_{50} of 0.07 mM), as shown evidently in the cellular morphology and in the DNA-stained nucleus. Only MCF7 cells exhibited apoptotic events upon AuNP treatment. AuNPs proved to

be safe as they are non-toxic against normal cells and myoblasts. Interestingly, the biosynthesized AuNPs were absorbed by the cells and are present in the cytosol, thus demonstrating selectivity toward breast and lung cancer cells used. The study showed the first evidence that AuNPs can be synthesized using lactic acid as a reducing agent and capping agent isolated from the probiotic *Lactobacillus acidophilus*. The results suggested potential cancer chemotherapeutic leads and targeted delivery in human breast and lung cancers.

KEYWORDS

cytotoxicity, lactic acid, cellular uptake, *Lactobacillus acidophilus*, nanotoxicity

Introduction

Cancer poses a significant public health problem as it is the second major cause of death worldwide. Breast cancer is the second most common cancer in women and the most diagnosed cancer in men. Lung cancer is the most common cancer death in both men and women (Siegel et al., 2022), with figures anticipated to climb in the coming years. Adjuvant radiation and chemotherapy, in combination with surgery, can help patients live longer. However, the abovementioned typical treatments have shortcomings, such as drug resistance and harmful effects from non-targeted drug distribution (Nurgali et al., 2018; Yao et al., 2020).

Nanotechnology has been widely gaining attention in medicine in recent decades, with applications for green technology, safer and more effective tumor diagnostics, treatment, and targeting. Nanoparticles can be generated from extremely small ionic metals and converted into nanoparticle material using various chemical synthesis methods. In contrast, compounds that are very large are converted into nanoparticle materials using a variety of physical and chemical procedures (Dang & Guan, 2020). The organic compounds used to reduce ionic metals are those that contain two or three carbon atoms with hydroxyl functional groups attached to them, examples of which are citric acid and lactic acid.

Drug delivery methods based on nanoparticles (NPs) have proven to offer several advantages in cancer treatment, including good pharmacokinetics, specific tumor cell targeting, reduced side effects, and drug resistance (Dang & Guan, 2020; Yao et al., 2020). The size and properties of NPs utilized in drug delivery systems are usually generated or chosen based on the pathophysiology of malignancies. Nano-carriers in cancer therapy target tumor cells mechanically by combining the carrier action of NPs with the positioning impact of the targeting chemical after absorption. They then provide medications to tumor cells to kill them. Traditional chemotherapy chemicals and nucleic acids are found on the inside of the nano-carriers, indicating that they could be used for both cytotoxic and gene therapies (Gavas et al., 2021). Furthermore, for some poorly soluble medicines, NPs provide a substrate for encapsulation and delivery into circulation (Gavas et al., 2021). Nano-carriers can enhance the half-life of pharmaceuticals and cause their accumulation in tumor tissues due to their size and surface features, as well as their role in boosting permeability and retention (Yao et al., 2020; Lei et al., 2022). Meanwhile, the targeting system safeguards normal cells from drug cytotoxicity, reducing the side effects of cancer treatment.

NP medicines have been used in cancer immunotherapy and ablation treatment, in addition to chemotherapy and gene therapy (Park et al., 2018; Thakur et al., 2020). The nanoparticle-based drug delivery technology is thought to enhance immunotherapy and counteract the immunosuppressive milieu found in tumors (Park et al., 2018; Thakur et al., 2020). Being widely used in biomedicine, toxicity assays must be performed to evaluate the effect of the nanomaterials on the host organism. *In vitro* biotoxicity assay using primary and cultured cell lines was the most feasible way to test the toxicity of nanomaterials on the host organism. *Lactobacillus spp.* has been used as a reducing and capping agent for the fast and efficient production of silver nanoparticles (Sintubin et al., 2009). To date, it has not been used to synthesize gold nanoparticles. This study aims to synthesize AuNPs by reducing chloroauric acid with lactic acid produced by *Lactobacillus acidophilus*, characterize the biosynthesized AuNPs, and determine their cytotoxicity against human breast and lung cancer cells, assessing their potential use in the biomedical field.

Materials and methods

Bacterial culture and lactic acid isolation

Lactobacillus acidophilus (USTCMS 1053) was cultured in a modified selective medium de Man, Rogosa, and Sharpe (MRS) agar and MRS broth. The culture was incubated in 100 mL of culture medium maintained in an anaerobic condition and incubated for 48 h. The bacterial biomass was separated from the culture medium *via* centrifugation at 3,000 rpm. The lactic acid in the culture medium was isolated by precipitation using calcium chloride dihydrate. The precipitated lactic acid was lyophilized, and its weight was determined before experimentation. Bruker Alpha II Fourier Transform Infrared (FTIR) spectrometer was used to determine the functional groups in the isolated lactic acid from 4,000 cm^{-1} to 400 cm^{-1}.

Biosynthesis of gold nanoparticles

A measure of 5 mL of diluted chloroauric acid (7 mM) was mixed with 1 mL of distilled water and 5 mL of 1.25 mg/mL calcium lactate isolated from *Lactobacillus acidophilus*. The mixture was adjusted to different pH values (pH 2, pH 5, and pH 8) and boiled for 3 min taking note of its color change. The absorbance of biosynthesized AuNPs at different pH ranges was scanned at 450–700 nm.

Characterization of biosynthesized gold nanoparticles

Characterization of biosynthesized AuNPs was sent for analysis to the Department of Science and Technology (DOST)–Industrial Technology Development Institute (ITDI)–Advanced Device and Materials Testing Laboratory (ADMATEL) for surface imaging and elemental analysis.

Sample preparation

One sample drop was cast, spread, and flattened on an aluminum foil. The sample in the foil was then stored and dried in a glass Petri dish with desiccant overnight and under a dark environment with 50 ± 10% relative humidity and 20–25°C temperature.

Surface imaging and elemental analysis

The sample was loaded and analyzed based on the instrument's operation manual. Surface imaging by field emission scanning electron microscopy (FESEM) and elemental analysis by energy-dispersive x-ray spectroscopy (EDS) were performed using the Dual Beam Helios NanoLab 600i system. The parameters used in the analysis were 10.0 kV accelerating voltage for the circular backscatter detector (CBS) of FESEM and 15.0 kV accelerating voltage for EDS with a beam current of 0.17 nA for CBS (FESEM) and 0.69 nA for EDS. Data processing and analysis of the FESEM image and elemental analysis (EDS) were performed using the Dual Beam Helios NanoLab 600i xT Microscope Server (FESEM) and Oxford EDS AZtecEnergy.

Atomic force microscopy (AFM) studies were performed in ambient conditions by NX-10 (Park Systems) in the non-contact mode. The sample was scanned at a rate of 0.76 Hz. The amplitude and point were set at 15.043×10^3 nm and 9.7472×10^3 nm, respectively. The frequency used was 290.83×10^3 Hz. The AFM instrument was housed in the Analytical Services Laboratory (ASL) in the Research Center for Natural and Applied Sciences (RCNAS).

Particle size distribution

Particle size analysis and distribution were determined using a CBS-mode image with evident black-and-white contrast of nanoparticles. The nanoparticle size was analyzed by ImageJ software, following the Feret diameter method and by interpreting using the frequency data.

Toxicity analysis of biosynthesized AuNPs

Cell lines were cultured in Dulbecco's minimum essential medium (DMEM) supplemented with fetal bovine serum (FBS), streptomycin, and penicillin. All cells were incubated in a humidified incubator at 37°C and 5% CO_2. Before assay, cells were grown at 1.0×10^4 cell density, seeded into a 96-well plate with desired media, and incubated for 24 h. Biosynthesized AuNPs were purified by centrifugation at 7,000 x g for 15 min and were re-dissolved in distilled water. After incubation, cells were treated with biosynthesized AuNPs and standard drugs and incubated for 48 h. After treatment, the media were removed and washed with phosphate-buffered saline, pH 7.0, (PBS) before analysis. PBS was removed and replaced with 20 µL of 3-(4,5-dimethylthiazol-2-yl)-2,5-diphenyl tetrazolium bromide (MTT) reagent and incubated for 4 h. A measure of 200 µL of dimethyl sulfoxide (DMSO) was added to each well containing the MTT reagent, and absorbance was read at 570 nm. The analyses were performed in triplicates, and the absorbance of untreated and treated cells was noted for the computation of cell viability or cytotoxicity. Mean and standard deviation were calculated, and one-way ANOVA was performed to compare the significance of the results.

The apoptotic potential of the biosynthesized AuNPs and the standard drug were also assessed with Hoechst 33342 for nuclear staining of the cells and caspase 3/7 (CellEvent Caspase 3/7 Green Detection Reagent, Thermo Scientific, United States) for the apoptosis caspase cascade signals. All cells were documented before and after treatment with MTT and Hoechst 33342 using an inverted light microscope (Evos FL Color, Invitrogen).

Results

Biosynthesis and characterization of lactate-capped AuNPs

In this study, gold nanoparticles were biosynthesized by reducing chloroauric acid using lactic acid isolated from *L. acidophilus*. To verify the identity of lactic acid isolated from *Lactobacillus acidophilus*, FTIR has been performed. Based on the IR spectra, we clearly observed the doublet peak at 3450 cm^{-1} due to -OH stretching near the methyl group and a strong, broad peak at 3100 cm^{-1} due to -OH stretching carboxylic acid. Moreover, there was a sharp, strong

peak at around 1600 cm^{-1} due to the C=O stretching of carboxylic acid. The sharp peak at around 1450 cm^{-1} and 1300 cm^{-1} can be attributed to the C-O stretching of the alcohol and carboxylic acid, respectively (Figure 1A). Peaks at approximately 1000 cm^{-1}, 980 cm^{-1}, and 700 cm^{-1} could be accounted for the presence of $CaCO_3$, CaO, and $Ca(OH)_2$ as by-products when isolating lactic acid from *Lactobacillus acidophilus*, respectively. These peaks are in accordance with the results obtained from SEM-EDS.

AuNPs were synthesized at lower concentrations of chloroauric acid and higher concentrations of lactic acid at different pH conditions. With these conditions, theoretically, the AuNPs synthesized should be smaller but at a higher yield. One of the good observations in determining a successful synthesis of AuNPs was an observable change in color of the colloidal sample after the synthesis; the mixture of chloroauric acid (yellow solution, Figure 1B) with lactic acid and water was changed at different pH conditions such as pH 2, pH 5, and pH 8. Among the different pH conditions, only pH 5 and pH 8 change their color into a purple colloidal solution and light purple or light orange colloidal solution, respectively (Figure 1B), while at pH 2, there was no significant change in its color, and no colloidal particles formed (Figure 1B). It was also observed that the synthesized AuNPs at pH 8 formed an aggregation and settled at the bottom of the glass container.

The synthesized AuNPs at different pH conditions were subjected to absorbance spectra determination with a wavelength range of 450 nm–700 nm. Based on the absorbance spectra, the synthesis of AuNPs at pH 5 and pH 8 has been accomplished; there was no observable biosynthesis of AuNPs at pH 2, as seen in Figure 1B. It has been shown that at pH 8, the trend of absorbance decreased, while at pH 5, the absorbance spectra of the biosynthesized AuNPs demonstrated an absorbance peak ranging from 520 nm to 560 nm with a maximum absorbance of 0.116–0.118. This result conforms with other published data on the absorbance peak of the synthesized AuNPs, as seen in Figure 1B. The distinct peak in the absorbance spectra of the synthesized AuNPs with pH 5 at 520 nm–560 nm, as well as the observation of purple to the violet color of the colloidal solution, validates the successful biosynthesis of AuNPs.

Biosynthesized AuNPs, with lactic acid as reducing agents at pH 5 conditions, revealed that the nanoparticles were spherical in shape, which in other published articles, were referred to as nanoshells or nanospheres. Among all the fields scanned for FESEM, only spherical shapes were observed, as shown in Supplementary Figure S1. Based on the surface micrograph, it has been established that at a certain condition, biosynthesized AuNPs generated nanoshells or nanospheres. Analysis of the particle size of synthesized AuNPs showed that most of the nanoparticles are 9 nm in size, exhibiting a greater frequency of sizes at 6–12nm, as indicated in Figure 1C. Other sizes detected are 3 nm, 15 nm, 18 nm, 21 nm, 24 nm, 27 nm, and 30 nm; however, it was observed with lower frequencies (Figure 1C). Hence, the nanoparticles produced, ranging from 6 to 12 nm, were smaller than another reported nanoparticle size. The small particle size distribution (6–12 nm, Figure 1C) of the synthesized nanoparticles confirms their higher toxicity to certain cells due to their greater tendency to pass through the cell membrane *via* endocytosis.

Elemental analysis using EDS showed that most of the elements detected on the sample of AuNPs were mostly composed of chlorine (Cl), calcium (Ca), oxygen (O), and carbon (C), as shown in Figure 1D. A low percentage in terms of the weight of gold (Au) was detected in the sample (Figure 1D) since the concentration of chloroauric acid used for the synthesis of AuNPs was much diluted. Moreover, the synthesized AuNPs are few and limited, whereas the high abundance of the other elements is attributed to the precipitated lactic acid in the form of calcium lactate. Calcium lactate is composed of calcium, carbon, oxygen, and hydrogen elements, which accounts for the elements present in the data analysis. The elemental chlorine detected was attributed to the excess chloride when calcium lactate precipitated. Calcium chloride was used to precipitate calcium lactate, and there are chlorine atoms attached to a complex mixture of chloroauric acid, which was used for the synthesis of AuNPs. All the elements other than Au detected in the elemental analysis were due to the components of the reagents used in synthesizing AuNPs. The presence of a distinct peak of Au rendered its successful reduction to Au^0, which is crucial in the formation of the AuNP colloidal solution.

The surface morphology of the biosynthesized gold nanoparticles (AuNPs) has been characterized by atomic force microscopy. The size of the gold nanoparticles ranges from 3 to 15 nm, showing a 3-D image and line profile analysis in Figure 1E. This confirmed the size of the biosynthesized AuNPs observed *via* SEM (Supplementary Figure S1).

To assess the reliability and merit of the green synthesis employed, the stability of the biosynthesized AuNPs over a period of time has been investigated by obtaining the UV-Vis spectra and the maximum peak in the absorbance spectra. Repeatability has been established by performing measurements for 10 days, demonstrating an absorbance at 520 nm equal to 1.999 ± 0.147, with RSD = 7.31% (Figure 1F). To ascertain reproducibility, the absorbance reading at the maximum peak has been measured for 30 days, showing absorbance equal to 1.781 ± 0.092, with RSD = 5.16% (Figure 1G).

Cytotoxicity, apoptotic, and cellular uptake studies of AuNPs on human breast adenocarcinoma (MCF7) and human lung adenocarcinoma (A549) cells

Here, cell viability using MTT assay was used to evaluate mitochondrial functions by determining the capability of the mitochondria of a living cell to reduce the MTT dye (yellow color) into a formazan crystal product (blue to purple coloration). The soluble formazan product in an organic solvent was read at 570 nm. Based on our MTT results,

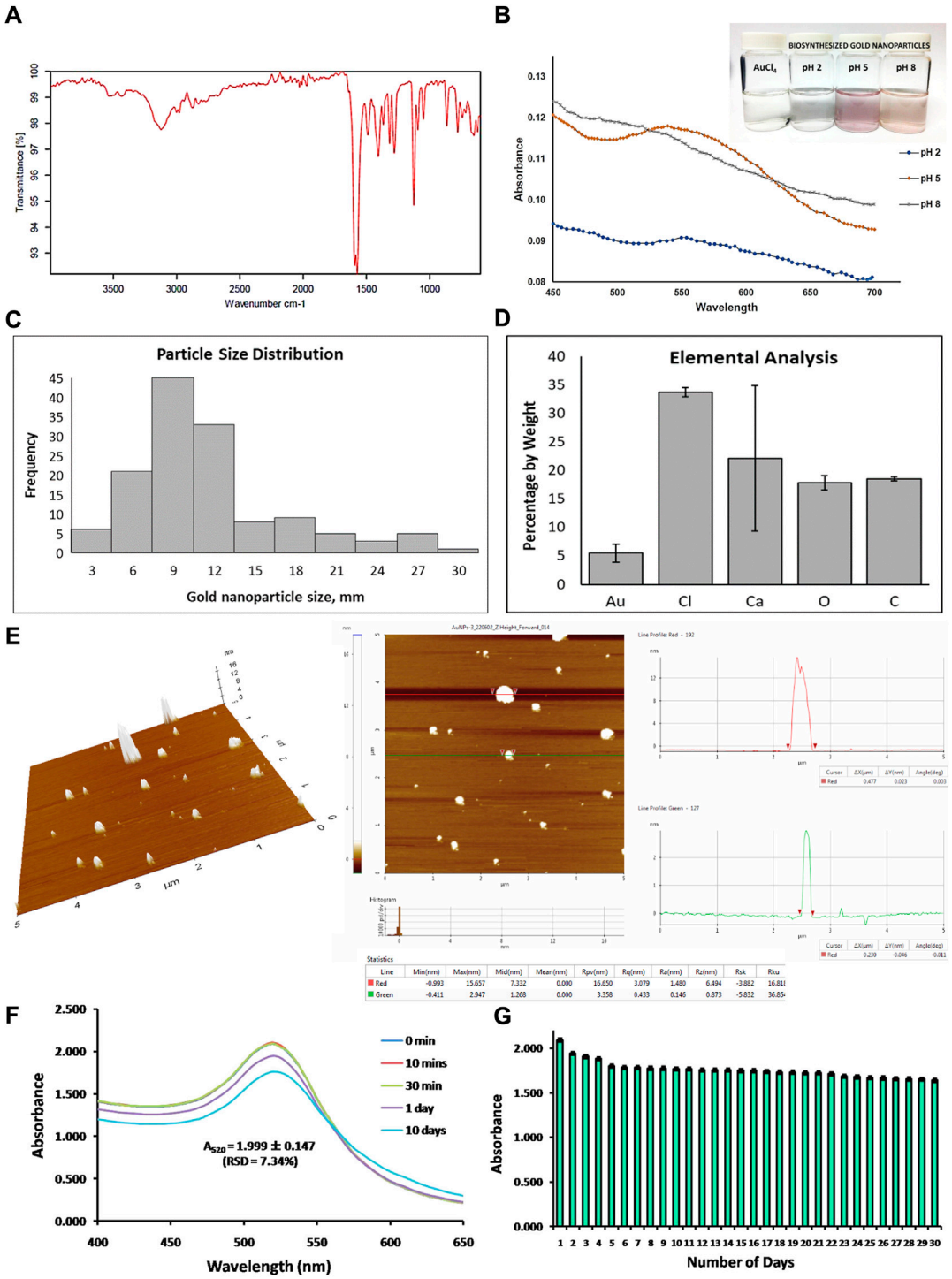

FIGURE 1
Characterization of biosynthesized gold nanoparticles from the reduction of chloroauric acid by lactic acid. **(A)** Characterization of lactic acid isolated from *Lactobacillus acidophilus* through its infrared spectra. **(B)** Analysis of absorbance data, wavelength spectrum, and visual appearance of biosynthesized gold nanoparticles at different pH conditions (pH 2, pH 5, and pH 8). **(C)** Particle size distribution determination in terms of nanometer (nm) scale, **(D)** elemental analysis of the sample in terms of percentage by weight of gold, chlorine, calcium, oxygen, and carbon detection, and **(E)** atomic force microscopic data analysis showing three-dimensional AFM images and line profile analysis of biosynthesized gold nanoparticles. Last, the stability of biosynthesized gold nanoparticles was analyzed **(F)** after 10 days of storage and **(G)** after 30 days of storage.

biosynthesized AuNPs showed a toxic effect on human breast cancer cells (MCF7) and human lung cancer cells (A549), as shown in Figure 2A. The toxicity of synthesized AuNPs was observed at 45–55% inhibition on the growth of both cell lines from 0.05 mM to 0.2 mM AuNP concentration (Figure 2A). It was also observed that there was low inhibition on the growth of normal cell lines (myoblasts) from 0.05 to 0.2 mM AuNP concentration (Figure 2A). The IC_{50} value of 0.075 mM of AuNPs against the human breast cancer cell line (MCF7) and the IC_{50} value of 0.07 mM of AuNPs for the human lung cancer cell line (A549) were computed. The selectivity index of biosynthesized AuNPs with MCF7 cells is 13.33, while with A549 cells is 14.29. Toxicity assessment based on the MTT assay, indicating mitochondrial metabolic impairment, showed that AuNPs are toxic to cancer cell lines on both MCF7 and A549. It has also been confirmed based on the cellular morphology of both cell lines using a bright-field inverted microscope (Figure 2B). Morphology of cells treated with different concentrations (0.05, 0.1, and 0.2 mM) of AuNPs showed that there was a detachment of the cells from the surface substrate, cell shrinkage, and a lesser number of cells in the field of vision, and some exhibited darkening of the cellular compartments, as seen in Figure 2B. Those characteristics of cells that were observed are part of being a toxic material that was being introduced into the cellular system.

Those characteristics that were observed under the microscope can be correlated with the result of the assay on metabolic impairment (MTT assay) since both data confirm that the AuNPs at 0.05–0.2 mM concentration could be toxic to the cancer cell lines (MCF7 and A549). Since the gathered data were limited to the assay performed, further analysis can be performed to determine the mechanism of cytotoxicity of biosynthesized AuNPs to cancer cells.

To evaluate nuclear membrane integrity and apoptosis, staining DNA was performed to check the possible effects of the synthesized AuNPs exhibited on both cancer cell lines (MCF7 and A549) (Figure 2B). The DNA-staining nuclear membrane analysis showed that the nuclear membrane of the cell lines (MCF7 and A549) treated with synthesized AuNPs was disrupted due to low and scattered blue fluorescent signals, and there is a decrease in the size of the nuclear compartment compared to the untreated cells. Also, some of the nuclei have undergone swelling since the blue fluorescent signals are being enlarged; some of the nuclei are merging, and some have fading blue fluorescent signals (Figure 2B). Nuclear membrane instability and disintegration of DNA of the cells are some reasons why the cells proceed to programmed cell death (apoptosis) or necrosis, depending on the macromolecular pathway that the cells are undergoing after being treated with synthesized AuNPs.

Apoptosis assay using caspase 3/7 assay detects caspase 3 and caspase 7 in cells based on their emission of green fluorescent signals. Among all the treated cancer cells (MCF7 and A549), only MCF7 cells treated with AuNPs showed green fluorescent signals, which means apoptosis only happened at that condition (Figure 2B).

After determining the effect of the synthesized AuNPs on the cancer cells (MCF7 and A549) in terms of their cytotoxic effect, DNA-stained nuclear membrane instability, and even their apoptotic effect on the cancer cells, the synthesized AuNPs were subjected to a cell uptake assay procedure to assess if the synthesized AuNPs are being taken up by the cells or they enter the cell by self-penetration due to their small size.

Cellular uptake has been observed using an inverted microscope. It was evident that the synthesized AuNPs are present in the cytosolic environment of the cells, and no trace of AuNPs' entry to the nucleus of the cells has been detected (Figure 2C). It was also established that there are more AuNPs found to be present in the cytosolic environment of human lung cancer cells (A549) (Figure 2C) than the AuNPs taken up by the human breast cancer cell line (MCF7) (Figure 2C).

Discussion

The biosynthesized gold nanoparticles used isolated lactic acid from *Lactobacillus acidophilus* as a reducing agent and capping agent. This proves to be a facile, green, and efficient approach for producing gold nanoparticles. Surface characterization such as SEM, EDS, and AFM has been performed to investigate the morphology of the biosynthesized AuNPs. Based on the results, spherical-shaped, with an average size of <15 nm AuNPs were synthesized, beneficial for health and biomedical applications. The stability of the biosynthesized AuNPs is evident through repeatability and reproducibility of the maximum absorbance in the UV-Vis spectra of the AuNPs within a 10-day and 30-day period, respectively. Absorbance at 520 nm equal to 1.999 ± 0.147, with RSD = 7.31% for repeatability was obtained. For reproducibility, the absorbance reading at the maximum peak for 30 days is equal to 1.781 ± 0.092, with RSD = 5.16%. With the stability, fine-tuned size, and shape of the AuNPs, target cancer cell lines such as MCF7 and A549 were investigated for cytotoxicity potential of the biosynthesized AuNPs.

In the extracellular matrix, cancer cells and non-malignant cells coexist. Acidity, hypoxia, hypertonicity, and stromal and immune cell recruitment are all characteristics of the tumor microenvironment. Low perfusion of aberrant vessels often inhibits both O_2 delivery and acidic waste product elimination by oxidative metabolism and the Warburg effect in the lung (Vanhove et al., 2019) and breast cancer (Kalezic et al., 2021) types. Furthermore, the spaces in the endothelium lining of cancer capillaries are excessive (varying from one to hundreds of nanometers), and AuNPs can easily extravasate through these spaces, demonstrating the tumor microenvironment's enhanced permeability and retention (EPR). Furthermore, the EPR effect allows nanoparticles to accumulate and permeate into tumors passively and preferentially, and

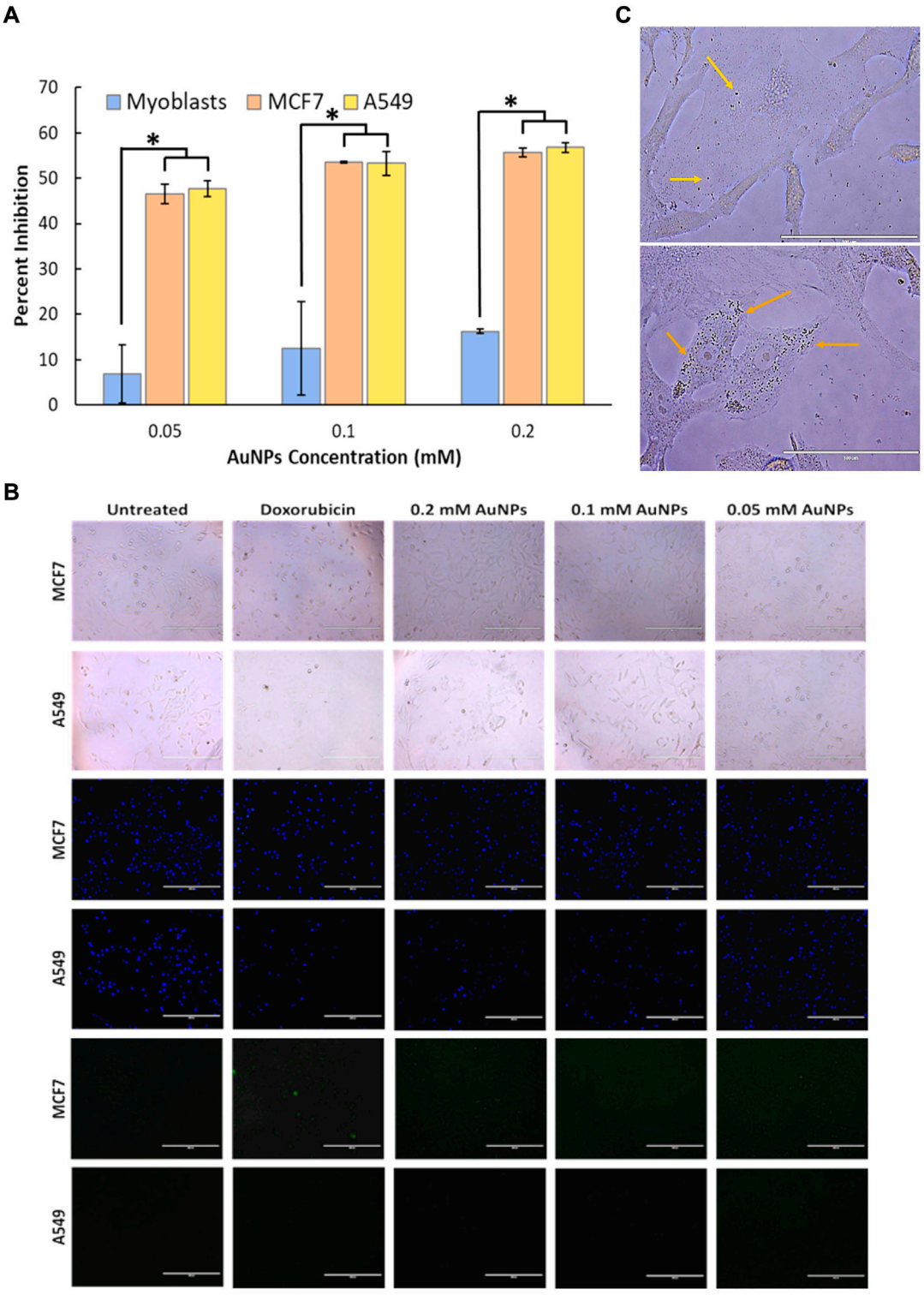

FIGURE 2
In vitro cytotoxicity analysis of **(A)** biosynthesized gold nanoparticles (0.05-, 0.1-, and 0.2-mM gold nanoparticle concentration) on normal cell lines (myoblasts) and cancer cell lines (MCF7 and A549). A significant difference between the treatment of cancer cell lines and normal cell lines was observed with a *p*-value less than 0.05, while no significant difference was observed within the treatment of cancer cell lines ($p > 0.05$). Cellular characterization on the effect of gold nanoparticles with 0.05-, 0.1-, and 0.2-mM concentrations in human breast cancer cells (MCF7) and human lung cancer cells (A549) through its **(B)** cellular uptake and localization on the cytosolic environment viewed under ×400 magnification, and its effect on **(C)** cell membrane morphology (bright field), DNA fragmentation (Hoechst 33324 dye), and apoptotic activity (Caspase 3/7).

nanoparticles can actively target cancer cell receptors by surface affinity ligand change (Gao et al., 2021).

The different characteristics of nanoparticles such as particle size, size distribution among the synthesized colloidal solution, particle shape, and surface are important determinants for their use in biomedical applications. Based on the surface micrographs from SEM studies, the particle size of the biosynthesized AuNPs was found to be ranging from 6 to 12 nm, with the highest particle size distribution of 9 nm. With their particle size, the biosynthesized AuNPs exhibited concentration-dependent toxicity against the MCF7 and A549 cells. Here, the cytotoxicity and mitochondrial membrane-damaging potential of the synthesized AuNPs against human breast (MCF 7) and lung (A549) cancer cells were analyzed relative to normal cells (myoblasts). MCF 7 and A549 cells are more sensitive to AuNPs than myoblasts and biosynthesized AuNPs, exhibiting suppressed cell growth in a concentration-dependent manner from 0.05 mM to 0.2 mM.

Using the Hoechst 33342 dye, changes in cellular and nuclear membrane shapes were detected, which were linked to AuNP cytotoxicity. MCF7 cells with apoptotic nuclei at 0.2 mM AuNPs had a unique marginated and fragmented appearance, which could be distinguished. The nuclei of control untreated cells were intact and normal. The findings imply that AuNPs' cytotoxicity was primarily due to a change in the mitochondrial function (MTT assay). However, the reduced viability of cells in the MTT assay revealed that AuNPs impaired cellular membrane integrity (Figure 2B). Changes in the phenotypic morphology of cells treated with nanomaterials are observed to occur by changing their morphological shape to rounded structures and losing cellular adhesion (Hanafy et al., 2020; Hanafy et al., 2021).

Among the AuNP treatment on the cancer cells, only MCF7 cells treated with AuNPs (0.05–0.2 mM) produced green fluorescence signals by caspase 3/7 fluorescent staining, indicating that apoptosis occurred only in that condition. Apoptosis induced by the caspase activity is driven by different pathways. Caspases are intracellular proteins activated for the programmed cell death or apoptosis of cells. One of the apoptotic pathways actively involved in apoptosis was the caspase cascade pathway. These caspases actively send signals into the mitochondria to produce cytochrome p450 and send signals to the nucleus for the breakdown of genetic data. Cell shrinkage, nuclear condensation, and increasing intensity of fluorescent signals are key factors in determining apoptotic progression. Deactivating mitochondrial membrane potential and activation of the caspase system contribute to the cytotoxic potential of the material (Hanafy et al., 2020; Hanafy et al., 2021).

In the study of Jawaid et al. (2020), small-size nanoparticles induced apoptotic activity through modified oxidative stress within the cells through the formation of reactive oxygen species, specifically the formation of intracellular superoxide and hydroxyl radicals. The formation of ROS in the cell leads to mitochondrial dysfunction, leading to the activation of caspase 3 following the caspase cascade pathway. The study of Kowsalya et al. (2020) also proves that even the biosynthesized gold nanoparticles using aqueous extracts from plant induces apoptotic activity against MCF7 breast cancer cells through the generations of intracellular ROS.

The interaction of nanomaterials with biological samples depends on their particle size. Decreasing the size of the materials increases the surface area of the nanoparticles, which increases reactivity with biological samples due to its interaction with the macromolecules and the cell system (Gatoo et al., 2014). Particle size can also influence the distribution of nanoparticles inside the cells; smaller nanoparticles enter the nucleus, whereas larger nanoparticles stay in the cytoplasm (Shang et al., 2014). Diverse particle size was produced at various methods of synthesis depending on different concentrations of chloroauric acid, reducing agents, and pH of the solution.

Spherical nanoparticles were more rapidly engulfed by the cell *via* phagocytosis or endocytosis than non-spherical nanoparticles, although being inherently more cytotoxic (Zhu et al., 2013). In this study, aside from the size of the biosynthesized AuNPs, their spherical structure contribute to the cellular uptake of the nanoparticles giving cytotoxic and apoptotic effects against the MCF7 and A549 cancer cells, as shown in Figure 2B.

In the study of Lunnoo et al. (2019), the cellular mechanism of how synthesized AuNPs were internalized across the cell membrane through *in silico* analysis and prediction has been reported. AuNPs' characteristics such as size, shape, surface charge, and aggregation contribute significantly to the endocytosis of the material. On the other hand, the complexity of the lipid bilayers in terms of lipid composition also affects endocytosis and the internalization rate. Based on the molecular dynamic simulation of Lunnoo et al. (2019), nano-spherical (10 nm, neutral) and nano-hexapod (2 nm, positively charged) AuNPs showed a faster rate of endocytosis and direct translocation through the plasma membrane due to their structure, size, and surface charges.

The gold nanoparticles extensively demonstrated a targeted delivery for cancer therapy. These nanoparticles have been widely used to deliver antitumor agents on the targeted site through enhanced permeability and retention effect (Paciotti et al., 2004; Arnida and Ghandehari, 2009). A unique phenomenon such as nanoparticle aggregation affects cellular uptake, cell health, and apoptosis when it is produced (Albanese & Chan, 2011). Assessing the cytotoxicity of nanoparticles can help improve its application for diagnostic imaging and therapeutic responses, as part of the contrast agents, as a drug carrier, or even as a drug itself (Albanese & Chan, 2011).

Conclusion

Biosynthesis of gold nanoparticles through the reduction of tetra chloroauric acid using the isolated lactic acid extract was

established. Based on FESEM with EDS and AFM, the biosynthesized AuNPs were found to be <15 nm and spherical-shaped. Cytotoxicity and apoptosis assay of the synthesized AuNPs showed that they are toxic against human breast adenocarcinoma cells (MCF7) and human lung cancer cells (A549). The nuclear damage was evident, but only MCF7 cells undergo apoptosis. AuNPs exhibited a non-toxic effect against myoblasts (normal cell line). Moreover, the biosynthesized AuNPs were found to be absorbed by the cells and to be present in the cytosolic environment of the cell. Hence, it can be said that the AuNPs exhibit selectivity in the toxicity effect against cell lines. The biosynthesized AuNPs were present in the cytosol, and their selectivity toward cancer cells can be optimized for their potential use in biomedical research on cell biology, cancer therapy, and targeted drug delivery.

For further studies, the mode of cell death and other mechanistic pathways of toxicity and cell–cell interaction are recommended to determine the effect of nanoparticles on the stage of the cell cycle and on the cell–cell interactions.

Data availability statement

The original contributions presented in the study are included in the article/Supplementary-Material further inquiries can be directed to the corresponding author.

Author contributions

All authors agree to be accountable for the content of this manuscript. ER, AC, and MD designed the analysis, collected the data, and wrote the methods, results, and discussion. MD and ME contributed data, performed the statistical analysis and the text mining analysis, and enhanced the results and discussion on biosynthesis and characterization of AuNPs. MS-B and MD facilitated the conception and design of the analysis, summarized the results, and discussed cytotoxicity, cellular uptake, and apoptosis of AuNPs on cells used. MD, ME, and MS-B revised and proofread the entire manuscript. All the authors have read and agreed to the published version of the manuscript.

Acknowledgments

The researchers would like to thank Mark Angelo Ngu, Alexis Labrador, Assoc. Prof. Felicidad Christina Ramirez-Peñafiel, Ph.D., and Prof. Christina Binag, Ph.D., for their significant contribution to this research, the UST Department of Biochemistry, and the UST Research Center for Natural and Applied Sciences for their support. They are also grateful to DOST-ITDI-ADMATEL for the sample analysis.

Conflict of interest

The authors declare that the research was conducted in the absence of any commercial or financial relationships that could be construed as a potential conflict of interest.

Publisher's note

All claims expressed in this article are solely those of the authors and do not necessarily represent those of their affiliated organizations, or those of the publisher, the editors, and the reviewers. Any product that may be evaluated in this article, or claim that may be made by its manufacturer, is not guaranteed or endorsed by the publisher.

Supplementary Material

The Supplementary Material for this article can be found online at: https://www.frontiersin.org/articles/10.3389/fmats.2022.933749/full#supplementary-material

References

Albanese, A., and Chan, W. C. W. (2011). Effect of gold nanoparticle aggregation on cell uptake and toxicity. *ACS Nano* 5 (7), 5478–5489. doi:10.1021/nn2007496

Arnida, A. M., and Ghandehari, H. (2009). Cellular uptake and toxicity of gold nanoparticles in prostate cancer cells: A comparative study of rods and spheres. *J. Appl. Toxicol.* 30 (3), 212–217. doi:10.1002/jat.1486

Dang, Y., and Guan, J. (2020). Nanoparticle-based drug delivery systems for cancer therapy. *Smart Mat. Med.* 1, 10–19. doi:10.1016/j.smaim.2020.04.001

Gao, Q., Zhang, J., Gao, J., Zhang, Z., Zhu, H., and Wang, D. (2021). Gold nanoparticles in cancer theranostics. *Front. Bioeng. Biotechnol.* 9, 647905. doi:10.3389/fbioe.2021.647905

Gatoo, M., Naseem, S., Arfat, M., Dar, A., Qasim, K., and Zubair, S. (2014). Physicochemical properties of nanomaterials: Implication in associated toxic manifestations. *Biomed. Res. Int.*, 1–8. doi:10.1155/2014/498420

Gavas, S., Quazi, S., and Karpiński, T. M. (2021). Nanoparticles for cancer therapy: Current progress and challenges. *Nanoscale Res. Lett.* 16 (1), 173. doi:10.1186/s11671-021-03628-6

Hanafy, N. A. N., Leporatti, S., and El-Kemary, M. A. (2021). Extraction of chlorophyll and carotenoids loaded into chitosan as potential targeted therapy and bio imaging agents for breast carcinoma. *Int. J. Biol. Macromol.* 182, 1150–1160. doi:10.1016/j.ijbiomac.2021.03.189

Hanafy, N. A. N., Leporatti, S., and El-Kemary, M. A. (2020). Mucoadhesive curcumin crosslinked carboxy methyl cellulose might increase inhibitory efficiency for liver cancer treatment. *Mater. Sci. Eng. C* 116, 111119. doi:10.1016/j.msec.2020.111119

Jawaid, P., Rehman, M. U., Zhao, Q. L., Misawa, M., Ishikawa, K., Hori, M., et al. (2020). Small size gold nanoparticles enhance apoptosis-induced by cold atmospheric plasma via depletion of intracellular GSH and

modification of oxidative stress. *Cell Death Discov.* 6, 83. doi:10.1038/s41420-020-00314-x

Kalezic, A., Udicki, M., Srdic Galic, B., Aleksic, M., Korac, A., Jankovic, A., et al. (2021). Tissue-specific Warburg effect in breast cancer and cancer-associated adipose tissue-relationship between AMPK and glycolysis. *Cancers* 13 (11), 2731. doi:10.3390/cancers13112731

Kowsalya, E., MosaChristas, K., Jaquline, C. R. I., Balashanmugam, P., and Devasena, T. (2020). Goldnanoparticles induced apoptosis via oxidative stress and mitochondrial dysfunctions in MCF-7 breast cancer cells. *Appl. Organomet. Chem.* 35, e6071. doi:10.1002/aoc.6071

Lei, W., Yang, C., Wu, Y., Ru, G., He, X., Tong, X., et al. (2022). Nanocarriers surface engineered with cell membranes for cancer targeted chemotherapy. *J. Nanobiotechnology* 20, 45. doi:10.1186/s12951-022-01251-w

Lunnoo, T., Assawakhajornsak, J., and Puangmali, T. (2019). *In silico* study of gold nanoparticle uptake into a mammalian cell: Interplay of size, shape, surface charge, and aggregation. *J. Phys. Chem. C* 123 (6), 3801–3810. doi:10.1021/acs.jpcc.8b07616

Nurgali, K., Jagoe, R. T., and Abalo, R. (2018). Editorial: Adverse effects of cancer chemotherapy: Anything new to improve tolerance and reduce sequelae. *Front. Pharmacol.* 9, 245. doi:10.3389/fphar.2018.00245

Paciotti, G. F., Myer, L., Weinreich, D., Goia, D., Pavel, N., McLaughlin, R. E., et al. (2004). Colloidal gold: A novel nanoparticle vector for tumor directed drug delivery. *Drug Deliv. (Lond).* 11 (3), 169–183. doi:10.1080/10717540490433895

Park, W., Heo, Y. J., and Han, D. K. (2018). New opportunities for nanoparticles in cancer immunotherapy. *Biomater. Res.* 22, 24. doi:10.1186/s40824-018-0133-y

Shang, L., Nienhaus, K., and Nienhaus, G. (2014). Engineered nanoparticles interacting with cells: Size matters. *J. Nanobiotechnology* 12, 5. doi:10.1186/1477-3155-12-5

Siegel, R. L., Miller, K. D., Fuchs, H. E., and Jemal, A. (2022). Cancer statistics, 2022. *Ca. A Cancer J. Clin.* 72 (1), 7–33. doi:10.3322/caac.21708

Sintubin, L., De Windt, W., Dick, J., Mast, J., Van Der Ha, D., Verstraete, W., et al. (2009). Lactic acid bacteria as reducing and capping agent for the fast and efficient production of silver nanoparticles. *Appl. Microbiol. Biotechnol.* 84, 741–749. doi:10.1007/s00253-009-2032-6

Thakur, N., Thakur, S., Chatterjee, S., Das, J., and Sil, P. C. (2020). Nanoparticles as smart carriers for enhanced cancer immunotherapy. *Front. Chem.* 8, 597806. doi:10.3389/fchem.2020.597806

Vanhove, K., Graulus, G. J., Mesotten, L., Thomeer, M., Derveaux, E., Noben, J. P., et al. (2019). The metabolic landscape of lung cancer: New insights in a disturbed glucose metabolism. *Front. Oncol.* 9, 1215. doi:10.3389/fonc.2019.01215

Yao, Y., Zhou, Y., Liu, L., Xu, Y., Chen, Q., Wang, Y., et al. (2020). Nanoparticle-based drug delivery in cancer therapy and its role in overcoming drug resistance. *Front. Mol. Biosci.* 7, 193. doi:10.3389/fmolb.2020.00193

Zhu, M., Nie, G., Meng, H., Xia, T., Nel, A., and Zhao, Y. (2013). Physicochemical properties determine nanomaterial cellular uptake, transport and fate. *Acc. Chem. Res.* 46 (3), 622–631. doi:10.1021/ar300031y